IMA Journal of Mathematics Applied in Medicine and Biology (2001) **18**, 263–292

Mathematical modelling of quorum sensing in bacteria

J. P. WARD†, J. R. KING AND A. J. KOERBER
Division of Theoretical Mechanics, School of Mathematical Sciences, University of Nottingham, Nottingham, NG7 2RD, UK

P. WILLIAMS
School of Pharmaceutical Sciences, University of Nottingham, Nottingham, NG7 2RD, UK

AND

J. M. CROFT AND R. E. SOCKETT
Division of Genetics, School of Clinical Laboratory Sciences, Queens Medical Centre, University of Nottingham, Nottingham, NG7 2UH, UK

[Received on 26 July 2000; revised on 13 July 2001]

The regulation of density-dependent behaviour by means of quorum sensing is widespread in bacteria, the relevant phenomena including bioluminescence and population expansion by swarming, as well as virulence. The process of quorum sensing is regulated by the production and monitoring of certain molecules (referred to as QSMs); on reaching an apparent threshold concentration of QSMs (reflecting high bacterial density) the bacterial colony in concert 'switches on' the density-dependent trait. In this paper a mathematical model which describes bacterial population growth and quorum sensing in a well mixed system is proposed and studied. We view the population of bacteria as consisting of down-regulated and up-regulated sub-populations, with QSMs being produced at a much faster rate by the up-regulated cells. Using curve fitting techniques for parameter estimation, solutions of the resulting system of ordinary differential equations are shown to agree well with experimental data. Asymptotic analysis in a biologically relevant limit is used to investigate the timescales for up-regulation of an exponentially growing population of bacteria, revealing the existence of bifurcation between limited and near-total up-regulation. For a fixed population of cells steady-state analysis reveals that in general one physical steady-state solution exists and is linearly stable; we believe this solution to be a global attractor. A bifurcation between limited and near-total up-regulation is also discussed in the steady-state limit.

Keywords: bacteria; quorum sensing; mathematical modelling; experimental validation; numerical solution; asymptotic analysis; steady-state analysis.

1. Introduction

It is well known that bacterial behaviour is very dependent on the environment, but only in recent years has it been discovered that the behavioural traits may vary dramatically with the population density (Fuqua *et al.*, 1996). This density-dependent behaviour was first

†Corresponding author. Email: john.ward@nottingham.ac.uk

observed about 30 years ago in a bioluminescent bacteria called *Vibrio fischeri* (Nealson *et al.*, 1970; Eberhard, 1972), which forms a symbiotic (mutually beneficial) relationship with certain species of squid. Here the squid provides nourishment for the bacteria to grow at certains sites on its body and the bioluminescence generated by the bacteria provides a means of communication between squid and may also mimic shimmering moonlight in the sea, thereby enabling the squid to evade attack by potential predators. In the case of *V. fischeri*, bioluminscence has a heavy energy demand and it is only worthwhile for the bacteria to produce light when they are at very high population densities, the light being too dim at low densities to promote symbiosis. It is observed, however, that at low population densities some individual bacteria may produce light, but at a relatively low intensity, and only at higher densities do they all apparently 'switch on' the genes concerned with bioluminescence. The understanding of the biochemical processes occurring in the regulation of density-dependent behaviour (known as quorum sensing) was greatly advanced following the discovery that a crucial signalling molecule, produced by *V. fischeri*, was involved (Eberhard *et al.*, 1981). Over the last 10 years or so, more and more species of bacteria have been discovered to employ a quorum sensing mechanism in controlling a wide range of behaviours (Fuqua *et al.*, 1996; Meighen, 1991; Swift *et al.*, 1996). Examples include production of a purple pigment by *Chromobacterium violeceum* (McClean *et al.*, 1997), increased motility and swarming in *Serratia liquefacians* (Eberl *et al.*, 1996), presumably to avoid the stresses of over-population, and induction of conjugal transfer (a form of sexual reproduction) in *Agrobacterium tumefacians* (Piper *et al.*, 1993). However, there are a number of more sinister examples of quorum sensing involving bacterial pathogenicity (Williams *et al.*, 2000). A well-studied example is *Pseudomonas aeruginosa*, which causes potentially fatal infections of immuno-compromised patients, particularly sufferers of cystic fibrosis (Doring, 1993) and those with severe burn injuries (Holder, 1993). On initial inoculation, this bacterium acts benignly at the injury site, increasing in population whilst remaining relatively unnoticed by the immune system. Eventually, at a high population density, the bacteria act in concert in switching on their virulence characteristics, releasing a cocktail of toxins and enzymes which destroy the host tissue, allowing infiltration and perhaps systemic infection (Rumbaugh *et al.*, 1999). The quorum sensing process enables *P. aeruginosa* to build up in density so that, at the time they become virulent, the immune system is more likely to be overwhelmed (Salmond *et al.*, 1995).

Quorum sensing bacteria determine their population density by the production, release and monitoring of one or more diffusible quorum sensing molecules (QSMs), the molecule(s) in question being dependent on the bacterial species. For example, for a large class of bacteria, namely Gram-negative species, the QSMs belong to a family of molecules known as *N*-acyl-homoserine lactones (Fuqua *et al.*, 1996; Swift *et al.*, 1996). As the population of bacteria increases so too does the QSM concentration, until some apparent threshold is reached at which all the bacteria switch on a behavioural trait; the population at this stage is sometimes referred to as being in a quorate state. On a more biochemical level, QSMs diffusing from the external media bind with an appropriate protein (QSP), located within the bacterium, to form a complex (see Fig. 1). This QSM–QSP complex in turn binds to a region of DNA on the bacterium's chromosome(s) (known as a *lux*-box), inducing or enhancing behavioural characteristics, as well as the up-regulation of QSM production (Swift *et al.*, 1996). In view of this self-induced up-regulation in QSM

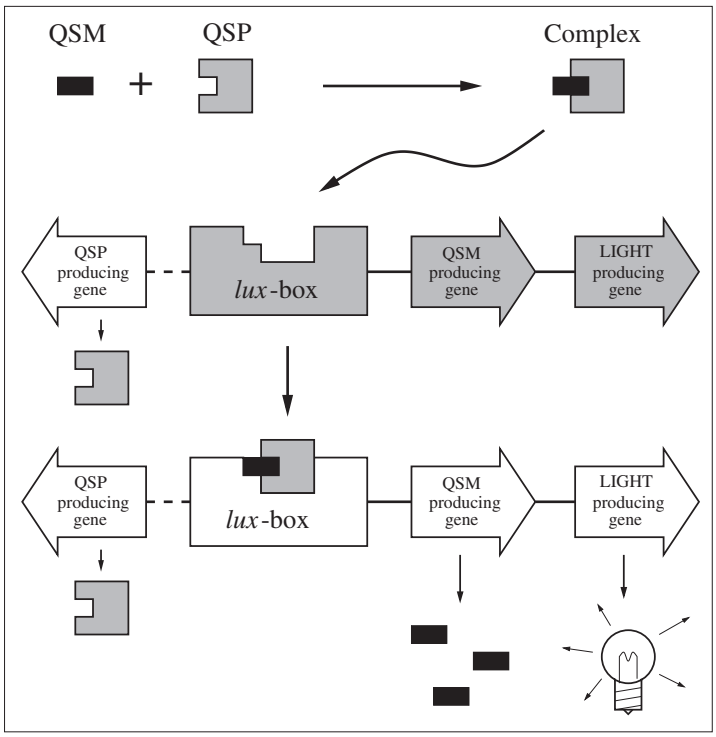

FIG. 1. Schematic illustration of the quorum sensing system of *V. fischeri*. QSM binds with the appropriate protein to form a complex which can then bind to the *lux*-box part of the quorum sensing gene region of the chromosome. The binding of the *lux*-box induces activation of the quorum sensing genes from a down-regulated state (grey background) to an up-regulated one (white background).

production, QSMs are often referred to as autoinducers. The *lux*-box bound QSM–QSP complex provides a stable base for the complexes involved in gene expression, namely RNA polymerase (RNAP), to activate the quorum sensing genes (Egland & Greenberg, 1999). However, even with an empty *lux*-box the RNAP can activate these genes, providing background production of QSMs, but this process is considerably more unstable. The system illustrated in Fig. 1, based on a schematic in Swift *et al.* (1996), represents the relatively simple quorum sensing process involved in bioluminescence in *V. fischeri*, for which there is only a single QSM. Our experimental work towards the verification of the model discussed in this paper focuses on *P. aeruginosa*, whose quorum sensing system is more complex, involving two or more QSMs. Here, the primary QSM, together with the primary QSP, up-regulates production not only of itself and some virulence factors, but also of the secondary QSM and QSP, the latter system being involved in the up-regulation of a number of other virulence factors (Swift *et al.*, 1996; McKnight *et al.*, 2000). The mathematical model introduced in this paper focuses on the production of a single QSM and is intended to be applicable not only to quorum sensing systems involving the production of only one QSM (e.g. *V. fischeri*) but also to the primary QSM of a multiple QSM quorum sensing system (e.g. *P. aeruginosa*).

The fact that quorum sensing in bacteria is a relatively recent discovery is reflected in the sparsity of existing mathematical models on the subject. Recently a model of regulation of bioluminescence in *V. fischeri* was proposed by James *et al.* (2000). They considered the model system illustrated in Fig. 1, focussing on the response of a single cell to external QSM concentrations. They derived a system of ordinary differential equations modelling the evolution of internal concentrations of QSM, QSP and QSM–QSP complex. This model predicts two stable steady states, corresponding to a non-bioluminescent state (zero QSM–QSP complex concentration) and a bioluminescent state (sufficiently high QSM–QSP complex concentration). More recently, Dockery & Keener (2001) modelled aspects of the basic biochemistry of the primary quorum sensing process of *P. aeruginosa*, based on mass action laws. They proposed that quorum sensing works by the switching between two stable steady-state solutions, reflecting relatively low and high rates of QSM production, whereby increasing the population density (which is treated as a parameter in their model) causes the shift from low to high production rates. In contrast to these models, that proposed in this paper couples cell population growth and QSM production and, rather than modelling the biochemistry of quorum sensing in detail, we focus on macroscopic features of external QSM concentrations (which are measurable) and sub-populations of down- and up-regulated cells.

The model described below treats the growth of a population of bacteria consisting of cells that are either up-regulated or down-regulated, the former producing QSM at a much faster rate than the latter. We assume that the growth medium is well mixed, resulting in a model consisting of a system of ordinary differential equations which is derived in the next section. The 'well mixed' assumption fits well with our experimental work involving colonies of cells grown in batch cultures, described briefly in Section 2.2, the results of which form the basis for the non-dimensionalization. Numerical solutions of the model are described and compared with experimental results in Section 3. In Section 4 asymptotic analysis is applied to the transient problem in order to determine timescales for the up-regulation of an exponentially growing colony which initially consists of down-regulated cells. In Section 5 we study steady-state solutions, corresponding to stationary phase of bacterial growth, and determine their linear stability.

2. Mathematical modelling

2.1 *The model*

Our modelling approach is to assume a well mixed population of cells, modelling cell growth and QSM production rate as a system of ordinary differential equations. For a bacterial population grown as a batch culture (see Section 2.2) the typical timescale for QSM concentrations to peak, often corresponding to maximal cell densities, is around 8–14 h for an initial low-density inoculum. The modelling assumptions can be summarized as follows.

- The model assumes that the population consists of up-regulated (density N_u, viewed as the number of cells per unit volume) and down-regulated (with density N_d) sub-populations of cells, corresponding to bacteria with a complex-bound or empty *lux*-box, respectively.

- We assume that down-regulated cells are up-regulated by QSMs (concentration A) with rate constant α. We note that the concentration of QSM A refers here to the external concentration. The QSM of *V. fischeri* is freely diffusible across the cell membrane (Kaplan & Greenberg, 1985); however, this is not the case for all quorum sensing bacteria. For example, the primary QSM of *P. aeruginosa* is not freely diffusible, but is biochemically pumped across the cell membrane, leading to differences in internal and external concentrations (Pearson *et al.*, 1999). However, the timescale for transport across the cell membrane to equilibrate is only about five minutes (Pearson *et al.*, 1999), much less than the timescales of interest, and hence we can assume that the internal and external concentrations are directly proportional; this partitioning in concentrations can be encompassed in the parameter α and the mathematical model is thus applicable to this case.
- The QSM is produced by both up-regulated and down-regulated cells, at rates κ_u and κ_d respectively, with $\kappa_d \ll \kappa_u$.
- Down-regulation occurs spontaneously, due to breakdown of *lux*-box bound QSM–QSP complex at a rate β.
- QSMs can be sequestered or broken down by the medium, and hence lost to the system, at a rate λ. The distinction between these two processes of QSM loss is not relevant in the current modelling.
- Cell division of up-regulated cells produces on average γ up-regulated and $2-\gamma$ down-regulated cells (where $0 \leqslant \gamma \leqslant 2$), assuming that only a proportion of replicated chromosomes contain occupied *lux*-boxes. We anticipate γ to be close to 1, corresponding to the division of an up-regulated cell producing one up-regulated and one down-regulated cell.
- Cell division of down-regulated cells produces two down-regulated cells.
- Cell-division rates of up-regulated and down-regulated cells are equal, being determined by the parameter r, where the doubling rate is $\ln(2)/r$ at low densities.

Applying these assumptions, we obtain the system of ordinary differential equations

$$\frac{\mathrm{d}N_d}{\mathrm{d}t} = r(N_d + (2-\gamma)N_u)F(N_d+N_u) - \alpha\, G(A)N_d + \beta N_u, \tag{1}$$

$$\frac{\mathrm{d}N_u}{\mathrm{d}t} = r(\gamma-1)N_u F(N_d+N_u) + \alpha\, G(A)N_d - \beta N_u, \tag{2}$$

$$\frac{\mathrm{d}A}{\mathrm{d}t} = \kappa_u N_u + \kappa_d N_d - \alpha\, G(A)N_d - \lambda A, \tag{3}$$

where $F(\cdot)$ is a suitable dimensionless bacterial growth function, with $F(0) = 0$, and the function $G(A)$ is discussed below. Equations (1)–(3) form a third-order system of nonlinear ordinary differential equations. The system can be simplified by considering the total density of bacterial cells ($N_T = N_d + N_u$), whereby adding (1) and (2) gives

$$\frac{\mathrm{d}N_T}{\mathrm{d}t} = rN_T F(N_T), \tag{4}$$

so that choosing $F(N_T) = 1 - N_T/K$, for example, gives logistic growth with carrying capacity K. In this paper we will assume for most part that $F(N_T)$ is continuous with a single positive zero $N_T = K$, where $F'(0) > 0$ and $F'(K) < 0$, so that $N_T = K$ is a stable and $N_T = 0$ an unstable steady state. Henceforth, we will focus on the variables N_T, N_u and A, noting that $N_d = N_T - N_u$.

The function $G(A)$ describes the overall process of QSM–QSP complex formation and *lux*-box binding, the units of which being QSM concentration. There are very few data in the literature that would indicate a suitable expression for $G(A)$ or, indeed, the relative concentrations of QSM and QSP within a cell. In this paper we assume $G(A)$ is linear, given by

$$G(A) = A, \tag{5}$$

which assumes that only a single QSM is involved in the QSM–QSP complex; the actual number being uncertain. This form of $G(A)$ is probably suitable for a developing colony, where the number of QSMs per cell is relatively small, and fits reasonably well with our experimental data. At high concentrations of QSM the up-regulation perhaps saturates so that Michaelis–Menten kinetics ($G(A) = A/(1 + k_a A)$), for example, may be more appropriate. Nevertheless, while including saturation leads to results that are qualitatively similar, the analysis is considerably more complicated, so in the absence of data to the contrary we adopt the simplest form for $G(A)$, given by (5).

2.2 *Parameter estimates and experimental work*

The assumption of a well stirred population of bacteria and uniform QSM concentration is well suited to bacterial growth in batch cultures whereby a colony is grown from a low initial inoculum in a flask containing a suitable liquid growth medium which is incubated in a cabinet at a constant temperature on a stage that rotates or vibrates. Our experiments (paper in preparation), specifically designed to give suitable parameter estimates, focus on growing several strains of *P. aeruginosa* in various media. These cultures were grown for up to 24 h at 37 °C and, at regular intervals, samples were taken to measure bacteria densities and QSM concentrations. QSM concentrations were determined using the *Eschercia coli* bioluminescent reporter strain (pSB1142), whereby the bioluminescence from the reporter strain grown in the super-natant from a batch culture is compared with that of media containing a known concentration of (synthetic) QSMs. Bacterial growth in batch cultures generally follows a standard pattern: usually there is an initial lag phase (1–2 h) followed by a 6–12 h phase of exponential growth until a limiting population density is reached, after which there is a phase in which the density remains roughly constant (the stationary phase). It is well known that the environmental stresses induced during the stationary phase lead to numerous changes in bacterial behaviour, including perhaps QSM production; however, we note that typically the population becomes quorate during the exponential phase of growth (Nealson *et al.*, 1970; Williams *et al.*, 1992). Given the model's simplicity we avoid the complications of stationary phase by determining the parameter values from experimental data obtained during exponential growth phase (during which $F(N_T) \sim 1$ holds). We note that, due to limitations in the experimental techniques, there is a restriction on the number of data points, usually between 7 and 10, that can be measured over the relevant

TABLE 1 *Parameter values determined using the curve fitting procedure on experimental data from batch cultures of P. aeruginosa. The values marked with ‡ indicate the range in which the sum of squares lies within approximately* 1% *of the minimum value*

		Growth medium	
Parameter	Units	20% serum solution	Standard laboratory broth (LB)
K	Cells ml^{-1}	3×10^9	5×10^{10}
r	1 h^{-1}	0·60	0·92
κ_u	1 h^{-1}	74 000	370 000
κ_d	1 h^{-1}	500	<1000 ‡
α	ml h^{-1} molecule^{-1}	8×10^{-11}	1×10^{-12}
β	1 h^{-1}	600	<100 ‡
λ	1 h^{-1}	1.5	0
γ	No units	1	0·9–1·5‡

time period. In order to determine best-fit parameter values, using the procedure described below, we should ideally have more data points. However, although qualitative agreement between experiments using the same growth medium is observed, quantitative consistency is very much more difficult to attain. There are a number of reasons for this, including slight variations in the growth media and in the state of the bacteria within the initial inoculum. Because of such variations, it is not in any case possible to determine robust parameter values, though their orders of magnitude can be reliably estimated.

Values for K and r can be determined by examination of the growth curve, while the QSM decay rate, λ, has been determined via independent experiments involving time course measurements of QSM added to fresh media. To obtain estimates of the remaining parameters (as well as suitable initial conditions) from the experimental data in a systematic way, we used an iterative curve-fitting procedure coupling numerical solutions of (2)–(4) with a least-squares fitting method. The differential equations were solved using the Numerical Algorithms Group (NAG) routine D02EJF, which uses a backward differencing technique. The least-squares procedure employs the public domain software MINPACK, which is a nonlinear least-squares package, based on the Levenberg–Marquardt algorithm, written by the Argonne National Laboratory.

Table 1 lists the parameter estimates for *P. aeruginosa* strain PAB1, a strain obtained from an infected burn wound, in two different growth media. The results in the table are representative of the variety of strains studied and demonstrate the range of variation of the results with different growth media; a full survey of best-fit parameter estimates are presented in Croft *et al.* (2000). The enhancement of growth and production rates in laboratorial broth (LB) over 20% serum (which is closer to a wound environment) is to be expected, in view of LB being specially prepared for promotion of bacterial growth. We note that the curve-fitting algorithm was most robust at determining values for κ_u and α; in general, 'best-fit' solutions for κ_d and β are more difficult to obtain reliably, since over a wide range of values there is very little deviation of the sum of squares from the minimum. The reasons for this are clarified below.

2.3 *Non-dimensionalization*

To determine the relative importance of the mechanisms involved in the model we non-dimensionalize the system of equations and exploit the parameter estimates given above. Denoting non-dimensional quantities with hats the variables are rescaled using

$$t = \hat{t}/r,\ N_u = K\hat{N}_u,\ N_T = K\hat{N}_T,\ A = \frac{\kappa_u K}{r}\hat{A},\ F(N_T) = \hat{F}(\hat{N}_T);$$

we note the rescaling implies that the population, when using a form for $F(N_T)$ which saturates, has carrying capacity $\hat{N}_T = 1$. Some of the analysis below considers exponential growth, i.e. $F(N_T) = 1$, in which case the K is assumed to be some representative population density. These rescalings result in the dimensionless system

$$\frac{\mathrm{d}\hat{N}_T}{\mathrm{d}\hat{t}} = \hat{N}_T\hat{F}(\hat{N}_T), \tag{6}$$

$$\frac{\mathrm{d}\hat{N}_u}{\mathrm{d}\hat{t}} = (\gamma - 1)\hat{N}_u\hat{F}(\hat{N}_T) + \hat{\alpha}\hat{A}(\hat{N}_T - \hat{N}_u) - \hat{\beta}\hat{N}_u, \tag{7}$$

$$\frac{\mathrm{d}\hat{A}}{\mathrm{d}\hat{t}} = \hat{N}_u + \varepsilon(\hat{N}_T - \hat{N}_u) - \hat{\mu}\hat{A}(\hat{N}_T - \hat{N}_u) - \hat{\lambda}\hat{A}, \tag{8}$$

where $\varepsilon = \kappa_d/\kappa_u$, $\hat{\alpha} = \alpha\kappa_u K/r^2$, $\hat{\beta} = \beta/r$, $\hat{\lambda} = \lambda/r$ and $\hat{\mu} = \alpha K/r$. Falling out naturally from the rescalings is the small parameter ε, which is the ratio of down-regulated to up-regulated cell QSM production rates. Of the remaining parameters the data $\hat{\alpha}$ is $O(10^4$–$10^5)$ being much the largest, with $\hat{\beta}$ being $O(10^2$–$10^3)$, $\hat{\lambda}$ being O(1) and $\hat{\mu}$ is relatively small $O(10^{-1})$. Simplifying the model by setting $\hat{\mu} = 0$ adds little in terms of tractability of the system, so the relevant term is kept for generality. We note that the data given in Table 1 is for a particular strain of *P. aeruginosa* in specific media. A change in media can give quite different values and perhaps result in significant differences in the magnitudes of the dimensionless parameters. For this reason the analysis of Sections 4 and 5 considers general values for the parameters, except that small $\hat{\varepsilon}$ is assumed throughout, with brief reference made to special cases inferred from the data. Henceforth, the hats will be dropped for clarity.

3. Numerical solution

In this section we examine numerical solutions to equations (6)–(8), comparing them to experimental data, and investigate the effects of varying some of the parameters over physically plausible ranges. The equations are solved using the NAG routine D02EJF.

Figures 2 and 3 show solutions using the best-fit parameter values for production in 20% serum (given in Table 1) during exponential growth of a colony, i.e. setting $F(N_T) = 1$, so that $N_T = N_t e^{rt}$ (with constant N_t) in (7) and (8). Reverting to dimensional quantities, Fig. 2 shows a log-plot of the evolution of QSM concentration in time together with the experimental the data to which it was fitted. We observe that the QSM concentration initially dips, then increases from about 3 h, at a rate which grows slightly faster than exponential, before retarding to steady exponentially growth. In this particular experiment a small amount of QSM was carried over with the inoculum

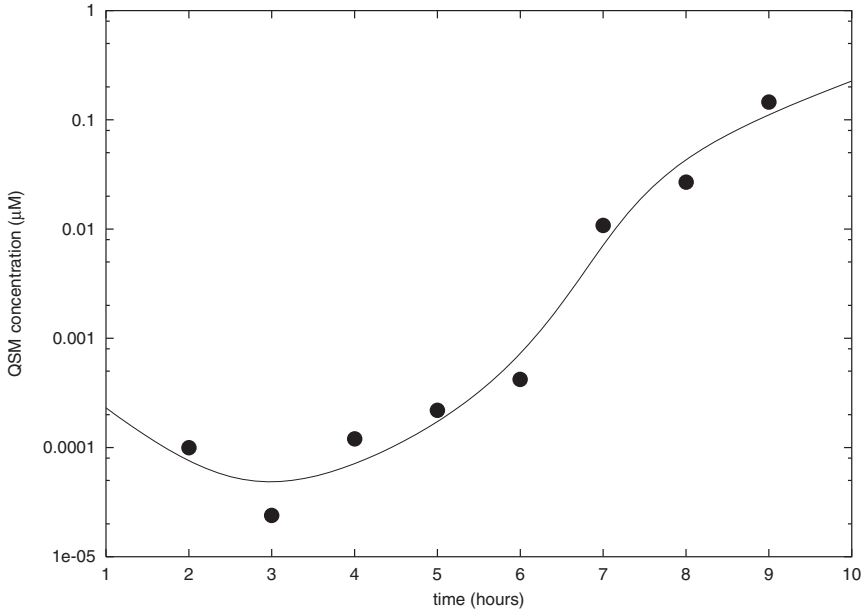

FIG. 2. Plot of QSM concentration against time, comparing model solution using best-fit parameters with experimental data of production in 20% serum (indicated by the • s). Note that we have reverted to dimensional quantities.

from the source culture; this is subsequently soaked up by the growth medium. During this period the exponentially increasing population of (mainly down-regulated) cells is producing QSM at a low rate, and not until about 3 h have passed there are sufficient cells to produce QSM faster than it is being soaked up. The gradual accumulation of QSM induces up-regulation of these down-regulated cells, most notably between 5–6 h (see Fig. 3), enhancing QSM production to a rate faster than $\exp(rt)$. Finally, when the vast majority of cells are up-regulated, so negligible further net up-regulation occurs, QSM production retards to $A \approx A_\infty \exp(rt)$ (for some constant A_∞), corresponding to the rate at which the population increases. This behaviour is clarified in the analysis of Section 4. The population beyond 10 h reaches a constant level and so too does the QSM concentration (not shown in the figure). For the reasons described in Section 2.2, the number of data points that can be recorded is limited, so it is possible that the final phase during which $A \approx A_\infty \exp(rt)$, is an artifact of the curve-fit and of the model, resulting from there being only three data points beyond the 7 h mark. Figure 3 demonstrates very well the quorum sensing phenomenon; note the rapid change of a colony from a down-regulated to an up-regulated state. Here, at 6 h very few cells are up-regulated, but beyond 8 h well over 90% have reached that state. In the case of the bioluminescent bacterium *V. fischeri*, this rapid jump to up-regulation would correspond to near-simultaneous initiation of light production by the entire population. In Section 4, timescales for these events are determined in the limit $\varepsilon \to 0$.

The effects of parameter α on the evolution of up-regulated cells and QSM

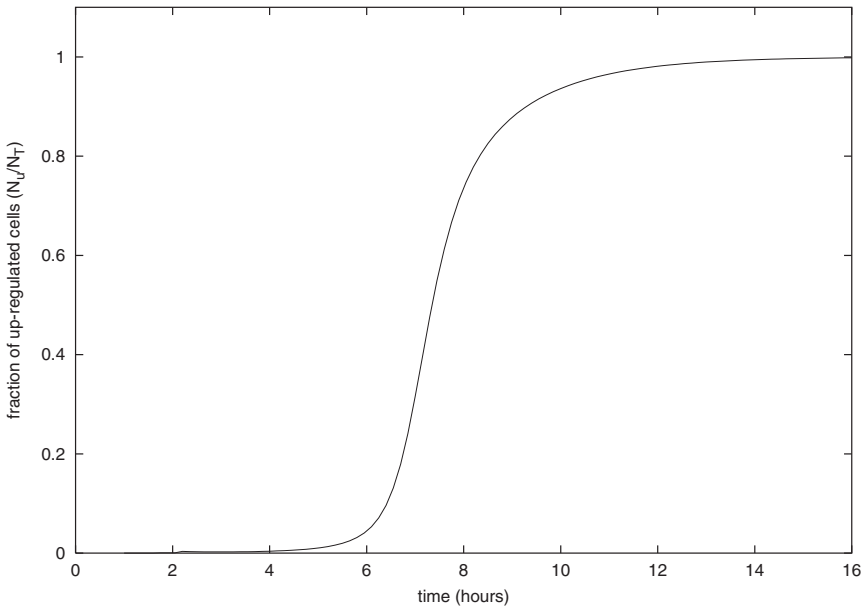

FIG. 3. Predicted evolution of the up-regulated cell fraction using the same best-fit parameters, listed in Table 1 (20% serum), as those used for Fig. 2.

concentration in an exponentially growing population are investigated in Figs 4 and 5. The parameters used are $\varepsilon = 0{\cdot}1, \mu = \beta = \lambda = \gamma = 1$ and $N_T(0) = 0{\cdot}1$, with the initial population consisting only of down-regulated cells. The parameter α governs the rate of up-regulation in the presence of QSM and, as expected, increasing α leads to faster and more enhanced up-regulation of the population. The figure shows that for $\alpha \geqslant 2$ the fraction of up-regulated cells tends to roughly unity, indicating near-complete up-regulation of the population; it is shown in Section 4 that $N_u/N_T \to 1$ as $t \to \infty$. We note that for large time the QSM concentration increases exponentially. For $\alpha < 2$, the ultimate fraction of up-regulated cells is less than one; for example, for $\alpha = 1$ less that 10% of the cells become up-regulated. In Fig. 5 we observe that, following an early transient, for $\alpha > 2$ the QSM concentration eventually settles to exponential growth, which is shown in the next section to be at the same rate as population growth (note that for long time, curves for $\alpha = 2{\cdot}2$ and $\alpha = 10$ are parallel). For $\alpha < 2$ the QSM concentration tends to a fixed level, corresponding to the fraction of up-regulated cells being less than unity. Eventual exponential growth is attained in the case $\alpha = 2$ but at a rate slower than population growth; in Section 4 it is shown that $A \sim A_\infty e^{\varepsilon\alpha t/\mu}$ holds as $\varepsilon \to 0$ and $t \to \infty$ at the relevant bifurcation point (for some constant A_∞). Such behaviour, shown in Figs 4 and 5, is explained in the next section where the bifurcation, in this case occurring at $\alpha = 2$, between exponential increase and eventual steady state of the QSM concentration is analysed in more detail.

The evolution of up-regulated cell fraction and QSM concentration for a logistically growing population of cells is shown in Fig. 6. Here, the parameter values are those for

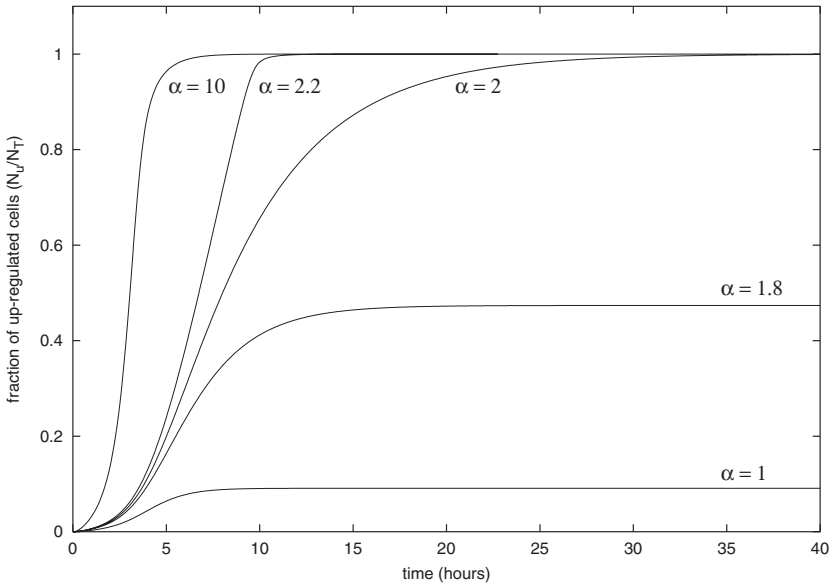

FIG. 4. The effects of α on the fraction of up-regulated cells for an exponentially growing bacteria population; $\alpha = 2$ is a bifurcation point.

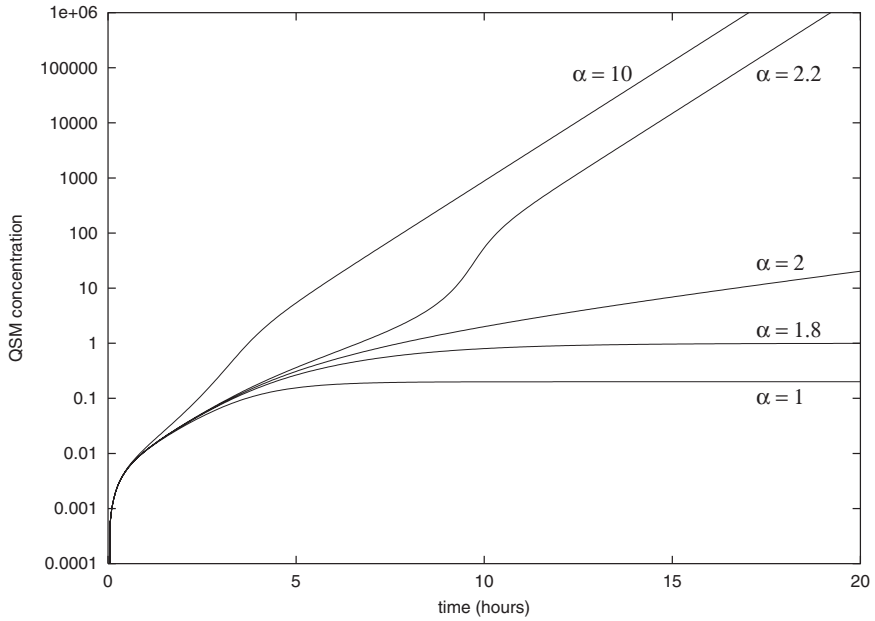

FIG. 5. The effects of α on the evolution of QSM concentration for an exponentially growing bacteria population; $\alpha = 2$ is a bifurcation point.

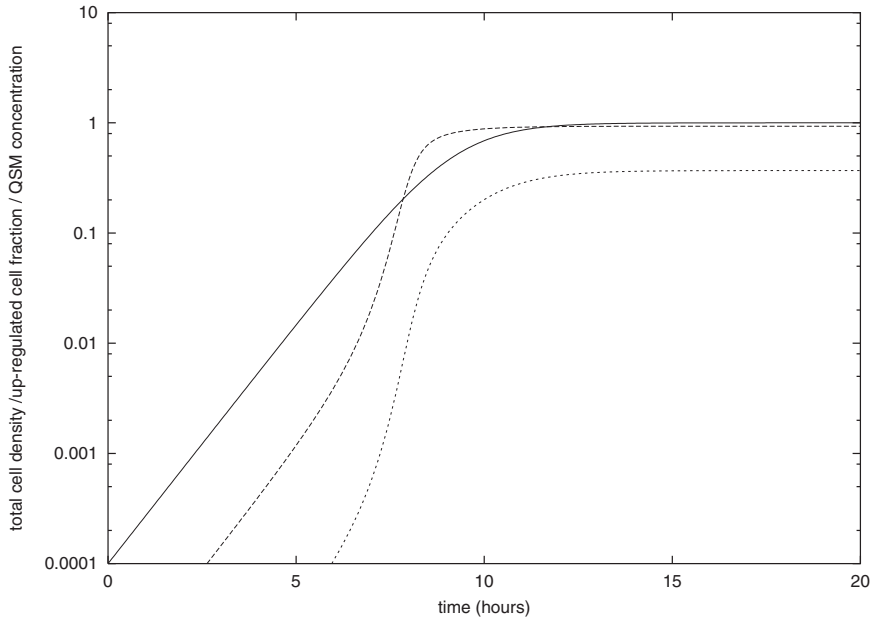

FIG. 6. Plot of the total cell density (solid), fraction of up-regulated cells (dashed) and QSM concentration (dotted), for cell population growth described by the logistic model.

20% serum given in Table 1. The figure shows the most rapid up-regulation occurs around 6–7 h, corresponding to the 'late' exponential phase of bacterial growth, i.e. shortly before the population reaches stationary phase. Such switching on of the quorum sensing process during the late exponential phase is observed in other quorum sensing systems, examples being *V. fischeri* (Nealson *et al.*, 1970) and *Erwina carotova* (Williams *et al.*, 1992).

The effects of the carrying capacity on the steady-state fraction of up-regulated cells and QSM concentration is shown in Fig. 7. The rest of the parameter values used are taken from the 20% serum data given in Table 1. We note that in the simulation to produce the curve the logistic model for growth was used; however, these steady-state solutions are independent of the precise form of growth expression, $F(N_T)$, used in (6). The figure demonstrates well the importance of population density for the quorum sensing process. To the left of the figure, where the final population is too small, there is insufficient accumulation of QSM to generate a significant population of up-regulated cells. Beyond a certain carrying capacity, however, almost total up-regulation always ensues. The carrying capacity in practice is dependent on numerous environmental factors, such as temperature, nutrient availability and pH.

4. Exponential growth: asymptotic analysis

4.1 *Scalings*

In this section we exploit the fact that ε is small to determine, in particular, the timescales involved for an exponentially growing population of down-regulated cells to become up-

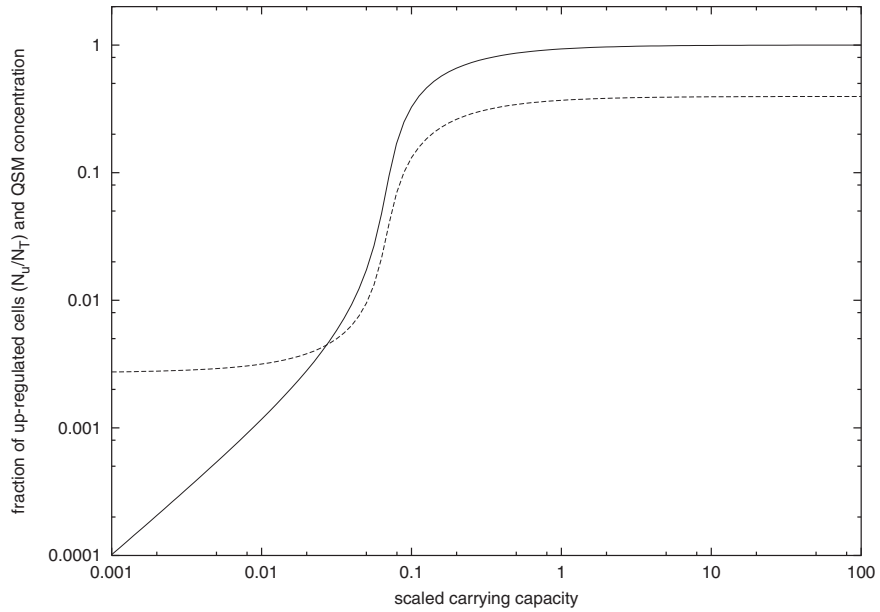

FIG. 7. The effect of the carrying capacity (scaled so that $K = 3 \times 10^9$ cells ml^{-1} corresponds to unity) on the steady-state fraction of up-regulated cells (solid curve) and QSM concentration (dashed curve).

regulated. This is particularly relevant biologically, as bacterial populations tend to become up-regulated (or quorate) during the exponential growth phase.

In the analysis below, we assume that the initial population of cells is of $O(\varepsilon)$, and there are no up-regulated cells or QSM present. The choice of initial conditions is of course somewhat arbitrary; however, the analysis below applies for arbitrarily small initial populations, though the length of the first timescale depends on the initial order of magnitude. Writing $N_T(0) = \varepsilon N_0$, the system of equations to be studied is

$$N_T = \varepsilon N_0 \, \mathrm{e}^t, \tag{9}$$

$$\frac{\mathrm{d}N_u}{\mathrm{d}t} = (\gamma - 1 - \beta)N_u + \alpha A(\varepsilon N_0 \, \mathrm{e}^t - N_u), \tag{10}$$

$$\frac{\mathrm{d}A}{\mathrm{d}t} = N_u + (\varepsilon - \mu A)(\varepsilon N_0 \, \mathrm{e}^t - N_u) - \lambda A, \tag{11}$$

subject to $N_u(0) = 0$ and $A(0) = 0$.

There are several timescales to be considered, depending on the value of the parameter Θ defined by (19) below. The main timescales that arise for various cases of Θ are now summarized.

$\Theta < 0$. There are two main timescales: (1) QSM production is predominantly by down-regulated cells with gradual up-regulation of a small proportion of cells (Section 4.2) and (2) the proportion of up-regulated (N_u/N_T) tends to a constant less than unity as $\varepsilon \to 0$ and $t \to \infty$ (Section 4.3.1).

$\Theta \geqslant 0$. There are three main timescales of interest: (1) is as for $\Theta < 0$, leading to a shorter timescale (2) in which the fraction of up-regulated is increasing rapidly (Section 4.3), leading to a final timescale (3) in which nearly all cells have become up-regulated. The details of the final timescale for $\Theta > 0$ and $\Theta = 0$ are different and are discussed separately in Sections 4.4 and 4.5 respectively.

The parameter value $\Theta = 0$ hence marks the bifurcation between a population becoming partially ($\Theta < 0$) or fully ($\Theta > 0$) quorate during the exponential growth phase.

4.2 $t = \mathrm{O}(1)$

On this timescale, QSMs are predominantly produced by down-regulated cells, and their concentration, as well as the up-regulated cell density, is very small. The appropriate scalings for this timescale are given by

$$t = \bar{t}, \quad N_u = \varepsilon^3 \bar{n} \sim \varepsilon^3 \bar{n}_0, \quad A = \varepsilon^2 \bar{a} \sim \varepsilon^2 \bar{a}_0,$$

giving the leading-order system

$$\frac{\mathrm{d}\bar{n}_0}{\mathrm{d}\bar{t}} = (\gamma - 1 - \beta)\bar{n}_0 + \alpha N_0 \bar{a}_0 \, \mathrm{e}^{\bar{t}}, \tag{12}$$

$$\frac{\mathrm{d}\bar{a}_0}{\mathrm{d}\bar{t}} = N_0 \, \mathrm{e}^{\bar{t}} - \lambda \bar{a}_0, \tag{13}$$

as $\varepsilon \to 0$, together with $\bar{n}_0(0) = 0$ and $\bar{a}_0(0) = 0$. These are easily solved to give

$$\bar{a}_0 = \mathrm{e}^{\bar{t}} \frac{N_0}{1 + \lambda} \left(1 - \mathrm{e}^{-(1+\lambda)\bar{t}}\right), \tag{14}$$

$$\bar{n}_0 = \mathrm{e}^{2\bar{t}} \begin{cases} \frac{\alpha N_0^2}{(1+\lambda)(3-\gamma+\beta)} \left(1 - \frac{3-\gamma+\beta}{2-\gamma-\lambda+\beta} \, \mathrm{e}^{-(1+\lambda)\bar{t}} + \frac{1+\lambda}{2-\gamma-\lambda+\beta} \, \mathrm{e}^{-(3-\gamma+\beta)\bar{t}}\right) & \beta \neq \lambda + \gamma - 2, \\ \frac{\alpha N_0^2}{(1+\lambda)(3-\gamma+\beta)} (1 - (3 - \gamma + \beta)\bar{t} \, \mathrm{e}^{-2\bar{t}} - \mathrm{e}^{-(3-\gamma+\beta)\bar{t}}) & \beta = \lambda + \gamma - 2. \end{cases} \tag{15}$$

In each of these solutions we have $\bar{n}_0$ growing as $\mathrm{e}^{2\bar{t}}$ and $\bar{a}_0$ as $\mathrm{e}^{\bar{t}}$ as $\bar{t} \to \infty$ and there is a shift in balance in (10) and (11) once N_u becomes the same order as A, namely when $t \sim \ln(1/\varepsilon)$. We note that α is typically large and the timescale on which the new balance occurs is given more accurately by a $t \sim \ln(1/\alpha\varepsilon)$.

A comparison of the QSM concentration predicted by the asymptotic analysis and a numerical solution of the full system is shown Fig. 8 (curve A). As expected, good agreement between the solutions occurs up to around $t = 3$, following which the solution of the next section becomes relevant.

4.3 $t = \ln(1/\varepsilon) + \mathrm{O}(1)$

4.3.1 $\varepsilon \to 0$. Although the density of up-regulated cells is very low compared with that of down-regulated ones, they are now producing QSM at a comparable rate. On this timescale the appropriate scalings are

$$t = \ln(1/\varepsilon) + \tilde{t}, \quad N_u = \varepsilon \tilde{n} \sim \varepsilon \tilde{n}_0, \quad A = \varepsilon \tilde{a} \sim \varepsilon \tilde{a}_0,$$

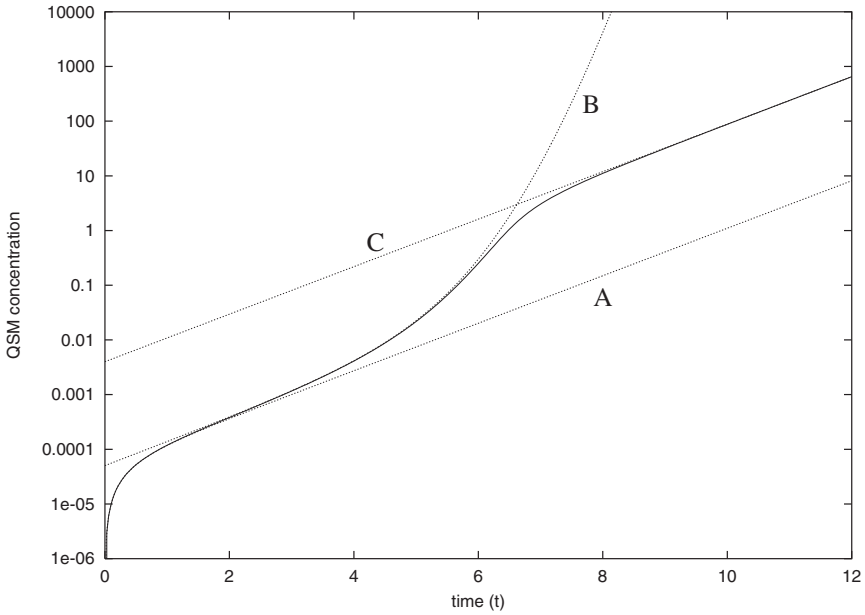

FIG. 8. Plot of QSM concentration against time, comparing the numerical solution (solid curve) with the asymptotic approximations (dotted curves) for each of the main timescales. The curves labelled A, B and C are the approximations on the $t = \mathrm{O}(1)$, $t \sim \ln(1/\varepsilon)$ (solving (16) and (17) numerically) timescales and in the limit $t \to \infty$, respectively; here we take $\varepsilon = 0{\cdot}01$, $\alpha = 10$, $\mu = \beta = \lambda = \gamma = N_0 = 1$ and $\Theta = 8$.

yielding at leading order

$$\frac{\mathrm{d}\tilde{n}_0}{\mathrm{d}\tilde{t}} = (\gamma - 1 - \beta)\tilde{n}_0 + \alpha N_0\, \tilde{a}_0\, \mathrm{e}^{\tilde{t}}, \tag{16}$$

$$\frac{\mathrm{d}\tilde{a}_0}{\mathrm{d}\tilde{t}} = \tilde{n}_0 + N_0 \mathrm{e}^{\tilde{t}} - (\mu N_0 \mathrm{e}^{\tilde{t}} + \lambda)\tilde{a}_0, \tag{17}$$

as $\varepsilon \to 0$, where by matching with the $t = \mathrm{O}(1)$ expansions we have $\tilde{n}_0(-\infty) = 0$ and $\tilde{a}_0(-\infty) = 0$. Equations (16) and (17) do not seem to be solvable in closed form, but in seeking large $\tilde{t}$ behaviour it is useful to consider the equation for $\tilde{n}_0$ derived by eliminating $\tilde{a}_0$, namely

$$\frac{\mathrm{d}^2\tilde{n}_0}{\mathrm{d}\tilde{t}^2} + (\mu N_0 \mathrm{e}^{\tilde{t}} + \beta + \lambda - \gamma)\frac{\mathrm{d}\tilde{n}_0}{\mathrm{d}\tilde{t}} - (\mu(\Theta + 1)N_0 \mathrm{e}^{\tilde{t}} - (1 - \lambda)(\gamma - 1 - \beta))\tilde{n}_0 = \alpha N_0^2 \mathrm{e}^{2\tilde{t}}, \tag{18}$$

where

$$\Theta = \frac{\alpha}{\mu} + \gamma - \beta - 2. \tag{19}$$

The relevance of Θ is made clearer by re-expressing it in terms of dimensional quantities, giving $\Theta = (\kappa_u + r(\gamma - 1) - \beta)/r$. Here, positive Θ implies that the rate of QSM

production exceeds the rate of down-regulation of up-regulated cells, that is to say that QSM production more than compensates for the amount consumed in restoring cells that have been down-regulated to an up-regulated state. Extracting the leading terms of (18) as $\tilde{t} \to \infty$ we have

$$\frac{\mathrm{d}\tilde{n}_0}{\mathrm{d}\tilde{t}} - (\Theta + 1)\tilde{n}_0 \sim \frac{\alpha}{\mu} N_0 \mathrm{e}^{\tilde{t}}, \tag{20}$$

from which we deduce that as $\tilde{t} \to \infty$

$$\tilde{n}_0 \sim \begin{cases} N_c \, \mathrm{e}^{(\Theta+1)\tilde{t}} & \Theta > 0, \\ \dfrac{\alpha}{\mu} N_0 \, \tilde{t} \, \mathrm{e}^{\tilde{t}} & \Theta = 0, \\ \dfrac{\alpha}{\mu \, (-\Theta)} N_0 \, \mathrm{e}^{\tilde{t}} & \Theta < 0, \end{cases} \tag{21}$$

where N_c is some constant determined by the evolution of the solution to (18) for $\tilde{t} = \mathrm{O}(1)$. Using (17), the corresponding behaviour of $\tilde{a}_0$ as $\tilde{t} \to \infty$ is given by

$$\tilde{a}_0 \sim \begin{cases} \dfrac{N_c}{\mu N_0} \, \mathrm{e}^{\Theta \tilde{t}} & \Theta > 0, \\ \dfrac{\alpha}{\mu^2} \tilde{t} & \Theta = 0, \\ \dfrac{\beta + 2 - \gamma}{\mu \, (-\Theta)} & \Theta < 0. \end{cases} \tag{22}$$

From these expansions it can clearly be seen that $\Theta = 0$ marks a bifurcation between exponential growth and levelling off of QSM concentration. For $\Theta > 0$, up-regulated cell growth is faster than population growth and there is a shift in balances in (10) and (11) when $\varepsilon \tilde{n} \sim \mathrm{e}^{\tilde{t}}$, i.e. when $\tilde{t} \sim \ln(1/\varepsilon)/\Theta$. For $\Theta = 0$ this shift in balance occurs on the timescale $\tilde{t} = \mathrm{O}(1/\varepsilon)$ timescale: this case is considered in Section 4.5. For $\Theta < 0$, (20) represents the leading-order balance for $t \to \infty$, there being no further timescale in this case, so we can deduce that for $\Theta < 0$

$$N_u \sim \frac{\alpha}{\mu \, (-\Theta)} N_T, \quad A \sim \varepsilon \frac{\beta + 2 - \gamma}{\mu \, (-\Theta)},$$

as $\varepsilon \to 0$ and $t \to \infty$.

The asymptotic solution for the QSM concentration on this timescale is compared with the numerical solution in Figs 8 and 9 (curves labelled B). In both cases the asymptotic expansions capture reasonably well the QSM concentration up to about in $t = 5$ in Fig. 8 and $t = 10$ in Fig. 9. In contrast, however, only in the former case do the solutions blend reasonably well in the overlap regimes. In Fig. 8, $\Theta = 8$ is relatively large and QSM production by up-regulated cells far exceeds binding in down-regulated cells, thereby producing up-regulation. In Fig. 9, we have $\Theta = 0{\cdot}5$, which is small. Here QSM production by cells is similar to consumption through up-regulation, so that the QSM level rises slowly over this timescale. Consequently, when the down-regulated cell density becomes very small compared with the overall population (at around $t = 13$; see Fig. 10, curve B) and consumption by down-regulated cells thus becomes negligible,

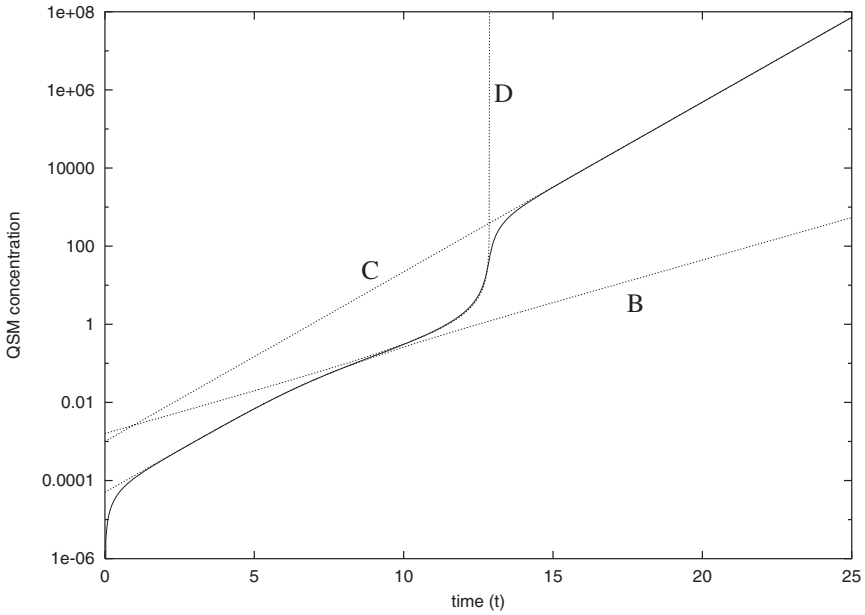

FIG. 9. Plot of QSM concentration against time, comparing the numerical solution (solid curve) with the asymptotic approximations (dotted curves). The curves labelled B, D and C are the approximations on the $t \sim \ln(1/\varepsilon)$ (solving (16) and (17) numerically), $t \sim \Theta \ln(1/\varepsilon)/(\Theta - 1)$ (solving (29)) and in the limit $t \to \infty$, respectively; here we take $\varepsilon = 0{\cdot}01$, $\alpha = 2{\cdot}5$, $\mu = \beta = \lambda = \gamma = N_0 = 1$ and $\Theta = 0{\cdot}5$.

there follows a short period of rapid accumulation of QSMs; this rapid rise is captured in the analysis of the next section. Figure 10, compares the asymptotic solutions to the numerically calculated down-regulated cell density, shown instead of the up-regulated cell density as it best illustrates the comparisons. The constant N_c was derived from matching with the numerical solution (here $N_c = 1{\cdot}6$) and we observe excellent agreement over much of the transition phase, i.e. over the $t \sim \ln(1/\varepsilon)$ timescale. An example with $\Theta < 0$ is shown in Fig. 11, the asymptotic solution being observed to capture well the $t = \mathrm{O}(1)$ and $t \to \infty$ timescales.

4.3.2 *The limit* $\Theta \to \infty$. The experimental data described in Section 2.2 suggest that α is large and μ is small, both corresponding to large Θ. In this section we briefly discuss the subsidiary limit $\mu \to 0$ (with α fixed) corresponding to $\Theta \to \infty$. The analysis for $t = \mathrm{O}(1)$ is unchanged; however with $\mu = 0$, (18) simplifies to

$$\frac{\mathrm{d}^2\tilde{n}_0}{\mathrm{d}\tilde{t}^2} + (\beta + \lambda - \gamma)\frac{\mathrm{d}\tilde{n}_0}{\mathrm{d}\tilde{t}} - (\alpha N_0 \mathrm{e}^{\tilde{t}} - (1-\lambda)(\gamma - 1 - \beta))\tilde{n}_0 = \alpha N_0^2 \mathrm{e}^{2\tilde{t}}, \tag{23}$$

subject to $\tilde{n}_0 \to 0$ as $\tilde{t} \to -\infty$. This equation can in principle be solved in terms of Bessel functions; however, it is more instructive to consider the limit $\tilde{t} \to \infty$. Applying the WKB

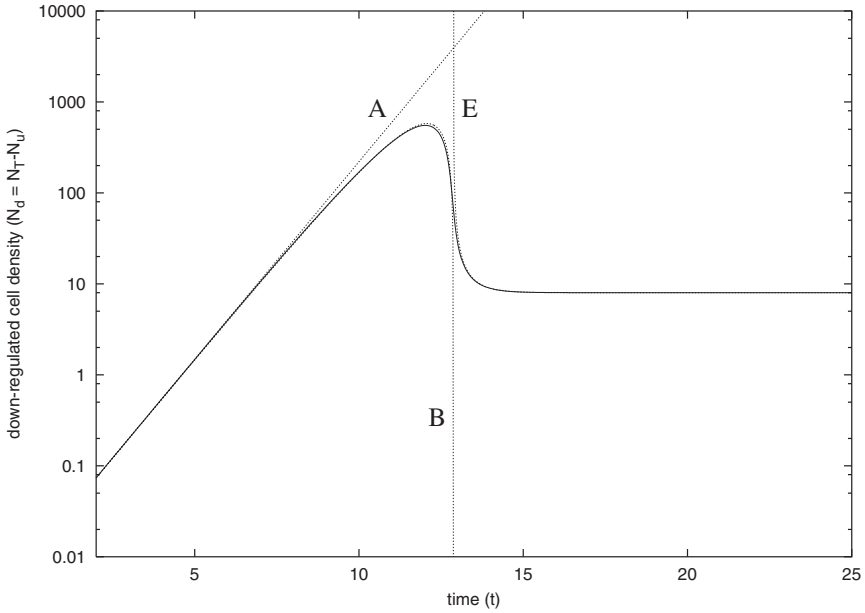

FIG. 10. Plot of down-regulated cell density against time, comparing the numerical solution (solid curve) with the asymptotic approximations (dotted curves). The curves labelled A, B and E are the approximations in the $t = \mathrm{O}(1)$, $t \sim \ln(1/\varepsilon)$ (solving (16) and (17) numerically) timescales and the final phase solution (38), respectively; here we take $\varepsilon = 0{\cdot}01$, $\alpha = 2{\cdot}5$, $\mu = \beta = \lambda = \gamma = N_0 = 1$ and $\Theta = 0{\cdot}5$.

method on (23) yields

$$\tilde{n}_0 \sim N_d \exp\left(2\sqrt{\alpha N_0}\, \mathrm{e}^{\tilde{t}/2} - \tfrac{1}{2}\left(\beta + \lambda - \gamma + \tfrac{1}{2}\right)\tilde{t}\right), \tag{24}$$

$$\tilde{a}_0 \sim \frac{1}{\sqrt{\alpha N_0}} \exp\left(2\sqrt{\alpha N_0}\, \mathrm{e}^{\tilde{t}/2} - \tfrac{1}{2}\left(\beta + \lambda - \gamma + \tfrac{3}{2}\right)\tilde{t}\right), \tag{25}$$

as $\tilde{t} \to \infty$ for some constant N_d. Two further timescales occur in the asymptotic analysis of (16) and (17) in the limit $\mu \to 0$, namely $\tilde{t} = \tilde{t}_{c_{1,2}}(\mu) + \mathrm{O}(1)$ with $\tilde{t}_{c_1} \sim \ln(1/\mu)$ and $\tilde{t}_{c_2} \sim 2\ln(1/\mu)$, in particular enabling the large $\tilde{t}$ asymptotic behaviour (20) and (21) to be recovered; the analysis relies on the WKB approach, the details of which are too complicated for the results to warrant further description. The crucial aspect of (24) is the much faster than exponential growth which features in this asymptotic regime.

4.4 $\Theta > 0$

4.4.1 $t = (\Theta + 1)\ln(1/\varepsilon)/\Theta + \mathrm{O}(1)$. On this timescale, the proportion of up-regulated cells and the QSM concentration become O(1). The appropriate scalings are

$$t = (\Theta + 1)\ln(1/\varepsilon)/\Theta + t^{\dagger} \quad , N_u = \varepsilon^{-1/\Theta} n^{\dagger} \sim \varepsilon^{-1/\Theta} n_0^{\dagger}, \quad A = a^{\dagger} \sim a_0^{\dagger}, \tag{26}$$

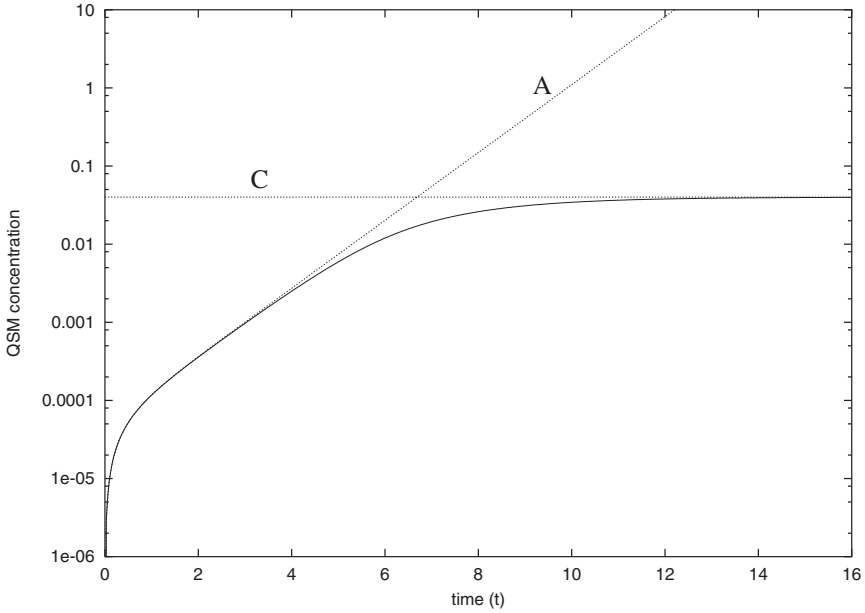

FIG. 11. Plot of QSM concentration against time, for the case $\Theta < 0$, comparing the numerical solution (solid curve) with the asymptotic approximations (dotted curves). The curves labelled A and C are the approximations on the $t = \mathrm{O}(1)$ timescale and as $t \to \infty$, respectively; here we take $\varepsilon = 0{\cdot}01, \alpha = 1{\cdot}5, \mu = \beta = \lambda = \gamma = N_0 = 1$ and $\Theta = -0{\cdot}5$.

for $\Theta > 0$. On substitution into (10) and (11) this yields

$$\frac{\mathrm{d}n_0^\dagger}{\mathrm{d}t^\dagger} = (\Theta + 1)n_0^\dagger, \tag{27}$$

$$a_0^\dagger = \frac{1}{\mu}\frac{n_0^\dagger}{(N_0 \mathrm{e}^{t^\dagger} - n_0^\dagger)}, \tag{28}$$

which by matching with (21) gives

$$n_0^\dagger = N_c \mathrm{e}^{(\Theta+1)\,t^\dagger}, \qquad a_0^\dagger = \frac{1}{\mu}\frac{1}{(N_0 \mathrm{e}^{-\Theta\, t^\dagger}/N_c - 1)} \tag{29}$$

for $\Theta > 0$. We observe from these expansions that N_u continues to grow faster than the N_T and that $a_0^\dagger$ blows up at a finite value of $t^\dagger$. Equation (29) was used to generate curve D in Fig. 9, capturing the rapid jump in QSM concentration; the value of the unknown constant N_c was again determined from the numerical solution for $\tilde{n}_0$ from the previous timescale. These expansions fail when $n_0^\dagger = N_0 \mathrm{e}^{t^\dagger}$ (when $a_0^\dagger$ blows up), leading to a further shift in balances between the terms of (10) and (11).

4.4.2 *The transition layer $t^\dagger = \mathrm{O}(1)$.* Before proceeding with the analysis we note that for $t^\dagger = \mathrm{O}(1)$ we have

$$\frac{\mathrm{d}n^\dagger}{\mathrm{d}t^\dagger} = (\gamma - 1 - \beta)n^\dagger + \alpha a^\dagger(N_0 \mathrm{e}^{t^\dagger} - n^\dagger), \tag{30}$$

$$\varepsilon^{1/\Theta}\frac{\mathrm{d}a^\dagger}{\mathrm{d}t^\dagger} = n^\dagger + (\varepsilon - \mu a^\dagger)(N_0 \mathrm{e}^{t^\dagger} - n^\dagger) - \varepsilon^{1/\Theta}\lambda a^\dagger, \tag{31}$$

so that

$$\frac{\mathrm{d}}{\mathrm{d}t^\dagger}(\mu n^\dagger + \alpha\varepsilon^{1/\Theta}a^\dagger) = \mu(\Theta + 1)n^\dagger + \varepsilon\alpha(N_0\mathrm{e}^{t^\dagger} - n^\dagger) - \varepsilon^{1/\Theta}\alpha\lambda\, a^\dagger. \tag{32}$$

The transition scalings resulting from the blow-up in (29) are

$$t^\dagger = t_c^\dagger(\varepsilon) + \varepsilon^{1/2\Theta}t^\ddagger, \quad n^\dagger = n_c^\dagger(\varepsilon) + \varepsilon^{1/2\Theta}n^\ddagger, \quad a^\dagger = a^\ddagger/\varepsilon^{1/2\Theta}, \tag{33}$$

where

$$t_c^\dagger(0) = \ln(N_0/N_c)/\Theta, \qquad n_c^\dagger(0) = N_0\mathrm{e}^{t_c^\dagger(0)}. \tag{34}$$

By suitable choice of the origin of $t^\ddagger$ and $n^\ddagger$ we then obtain from (30) and (32) that

$$\mu n_0^\ddagger + \alpha a_0^\ddagger = \mu(\Theta + 1)N_0\mathrm{e}^{t_c^\dagger(0)}t^\ddagger,$$

$$\frac{\mathrm{d}n_0^\ddagger}{\mathrm{d}t^\ddagger} = (\gamma - 1 - \beta)N_0\mathrm{e}^{t_c^\dagger(0)} + \mu((\Theta + 1)N_0\mathrm{e}^{t_c^\dagger(0)}t^\ddagger - n_0^\ddagger)(N_0\mathrm{e}^{t_c^\dagger(0)}t^\ddagger - n_0^\ddagger),$$

a Riccati equation which implies that

$$n_0^\ddagger \sim N_0\mathrm{e}^{t_c^\dagger(0)}t^\ddagger, \qquad a_0^\ddagger \sim \frac{\mu}{\alpha}\Theta N_0\mathrm{e}^{t_c^\dagger(0)}t^\ddagger, \tag{35}$$

as $t^\ddagger \to \infty$. This transition layer corresponds to the fast-turnaround phase appearing near the centre of the plots in Figs 8 and 9.

4.4.3 *The final phase.* Here we have $t^\dagger = \mathrm{O}(1)$ with $t^\dagger > t_c^\dagger$. The scalings are

$$n^\dagger = \check{n}, \quad a^\dagger = \varepsilon^{-1/\Theta}\check{a},$$

where from (30)

$$\check{n} \sim N_0\mathrm{e}^{t^\dagger} - \varepsilon^{1/\Theta}\check{n}_1, \tag{36}$$

indicating that nearly all cells have been up-regulated. The positive correction term $\check{n}_1$ is the leading-order density of down-regulated cells. Equation (32) yields

$$\frac{\mathrm{d}\check{a}_0}{\mathrm{d}t^\dagger} = \frac{\mu\,\Theta}{\alpha}N_0\mathrm{e}^{t^\dagger} - \lambda\check{a}_0,$$

so that

$$\breve{a}_0 = \frac{\mu\,\Theta}{\alpha(\lambda+1)} N_0 (\mathrm{e}^{t^\dagger} - \mathrm{e}^{(1+\lambda)t_c^\dagger(0)} \mathrm{e}^{-\lambda t^\dagger}), \tag{37}$$

thereby matching with (35); hence A also grows like e^t for large t. Using (37) the correction term $\breve{n}_1$ can be determined from (30), yielding

$$N_d \sim \breve{n}_1 = \frac{(\beta + 2 - \gamma)(1+\lambda)}{\mu\,\Theta\,(1 - \mathrm{e}^{-(1+\lambda)(t^\dagger - t_c^\dagger(0))})}, \tag{38}$$

hence the density of down-regulated cells tends to a fixed value as $t^\dagger \to \infty$.

The asymptotic solutions as $t \to \infty$ (37) agree well in both Figs 8 and 9 (curves C). Equation (38) is compared to the numerical solution in Fig. 10 (Curve E), where $t_c^\dagger$ was derived via (34) using the numerically determined value for N_c ($N_c = 1{\cdot}6$) from the previous timescale. We observe that the final-phase solution provides excellent agreement with the numerical solution beyond the transition phase.

4.5 $\Theta = 0$

For $\Theta = 0$ the relevant scalings on the third timescale change from (26) to

$$t = \ln(1/\varepsilon) + t^\dagger/\varepsilon, \quad N_u = \mathrm{e}^{t^\dagger/\varepsilon} n^\dagger, \quad A = a^\dagger.$$

To leading order (9) and (11) each yield

$$a_0^\dagger = \frac{1}{\mu} \frac{n_0^\dagger}{N_0 - n_0^\dagger}, \tag{39}$$

and from the correction terms we find that

$$\frac{\mathrm{d}n_0^\dagger}{\mathrm{d}t^\dagger} = \frac{\alpha}{\mu}(N_0 - n_0^\dagger),$$

so that (matching as $t^\dagger \to 0$)

$$n_0^\dagger = N_0(1 - \mathrm{e}^{-\alpha t^\dagger/\mu}), \qquad a_0^\dagger = (\mathrm{e}^{\alpha t^\dagger/\mu} - 1)/\mu. \tag{40}$$

In this case there is no further shift in balances to the system (9) and (11) so that

$$N_u \sim N_T(1 - \mathrm{e}^{-\varepsilon\alpha t/\mu}), \qquad A \sim \frac{1}{\mu}(\mathrm{e}^{\varepsilon\alpha t/\mu} - 1), \tag{41}$$

hold as $\varepsilon \to 0$ for sufficiently large t. Consequently, for large-time we have $N_u \to N_T$ with A growing exponentially, but much more slowly than the population growth; this non-generic large time behaviour occurs only at the bifurcation point. The $\Theta = 0$ case corresponds to the $\alpha = 2$ in Fig. 5 where the contrast over cases with $\Theta > 0$ cases is clearly observed.

5. Fixed population: steady-state analysis

5.1 *Introduction*

In the majority of batch culture experiments the population of cells become quorate, produce light in the case of *V. fischeri* or become virulent in the case of *P. aeruginosa*, during the exponential growth phase. In order to gain some insight into how this quorate population may develop into the stationary growth phase, we now investigate the existence and stability of steady-state solutions of the model, assuming a finite carrying capacity. The steady-state analysis below will reveal a bifurcation in the limit $\varepsilon \to 0$, similar to the bifurcation of the previous section, between negligible and O(1) levels of up-regulated cell fraction.

As described in Section 2.2 we assume that $F(N_T)$ has only one positive zero, at $N_T = 1$, which (since $F'(1) < 0$) represents a stable solution. We note that the analysis is tractable for all non-negative parameter values, but we include a few references to the limit $\varepsilon \to 0$.

5.2 *Steady-state solutions*

Setting the derivatives in (7) and (8) to zero, with $N_T = 1$, and imposing $F(1) = 0$ yields

$$0 = \alpha A^*(1 - N_u^*) - \beta N_u^*, \tag{42}$$

$$0 = N_u^* + (1 - N_u^*)(\varepsilon - \mu A^*) - \lambda A^*, \tag{43}$$

where the asterisks denote steady-state solutions. From (42) and (43) we have

$$A^* = \frac{N_u^* + \varepsilon(1 - N_u^*)}{\mu(1 - N_u^*) + \lambda} = \frac{\beta}{\alpha}\frac{N_u^*}{1 - N_u^*}, \tag{44}$$

whereby N_u^* satisfies the quadratic

$$p_2 N_u^{*2} - p_1 N_u^* - \varepsilon = 0, \tag{45}$$

where

$$p_1 = 1 - 2\varepsilon - \frac{\beta}{\alpha}(\mu + \lambda), \quad p_2 = 1 - \epsilon - \frac{\mu\beta}{\alpha}. \tag{46}$$

For the steady-state solutions to be physical we require $0 \leqslant N_u^* \leqslant N_T = 1$ and $0 \leqslant A^* < \infty$. The number of physical solutions is dependent on the values of p_1 and p_2, each of the cases being discussed below. Before proceeding with the analysis, we introduce the following parameter:

$$\Psi = \alpha - \beta(\lambda + \mu), \tag{47}$$

so that $p_1 = (\Psi - 2\varepsilon)/\alpha$, which is relevent to the bifurcation analysis described below. We note that positivity of Ψ implies that the up-regulation rate is faster than the rates of down-regulation of up-regulated cells and of QSM loss via cell up-regulation and via absorption by the external medium. We now first discuss briefly some of the more notable special cases, which give some insight into the behaviour in the limiting cases.

$\varepsilon = 0$. This is an unphysical case in which down-regulated cells are unable to produce QSM. However, it is also the only case in which there are two physical steady-state solutions, namely $N_u^* = 0$ and $N_u^* = \Psi/(\Psi+\beta\lambda)$, provided that $\Psi > 0$. For $\Psi \leqslant 0$ the only physical solution is the trivial state of $N_u^* = 0$.

$\lambda = 0$. In this case the only non-trivial (i.e. $N_u^* > 0$) solution for QSM concentration is given by $A^* = \varepsilon\beta/(\mu\beta - \alpha)$. For physical solutions we require $\alpha < \mu\beta$ (or $\Psi < 0$), implying that the rate of up-regulation must be sufficiently low, compared with QSM usage and *lux*-bound QSM–QSP complex breakdown, for there to be steady-state solutions. For the case $\alpha \geqslant \mu\beta$ (or $\Psi \geqslant 0$) there are no steady-state solutions and as $t \to \infty$ it can be shown that $A \sim (1 - \mu\beta/\alpha)\, t$ and $N_u = 1 - \mathrm{O}(1/t)$ for $\Psi > 0$ and $A \sim \sqrt{2\varepsilon/\mu}\, t^{1/2}$ and $N_u = 1 - \mathrm{O}(1/\sqrt{t})$ for $\Psi = 0$.

$\beta = 0$. Here there is no *lux*-bound QSM–QSP complex breakdown, so the physical solution corresponds to the population being completely up-regulated, $N_u^* = 1$. In this case $A^* = 1/\lambda$, implying an unbounded solution when $\lambda = 0$.

$\alpha = 0$. This is the trivial case of no up-regulation of cells and hence $N_u^* = 0$, yielding $A^* = \varepsilon/(\lambda + \mu)$.

Before discussing the various cases (depending on the sign of p_2), we note the following inequalities:

$$p_1^2 + 4\,\varepsilon p_2 = \left(1 - \frac{\beta}{\alpha}(\lambda+\mu)\right)^2 + 4\varepsilon\frac{\beta\lambda}{\alpha} \geqslant 0, \tag{48}$$

$$p_2 - p_1 = \varepsilon + \frac{\beta\lambda}{\alpha} \geqslant 0. \tag{49}$$

Equation (48) ensures that for all non-negative parameter values the solutions of (45) are real; (49) ensures in particular that if $p_2 = 0$ then $p_1 < 0$ and, from (45), there exists a positive solution for N_u^*. There are three cases to consider, namely $p_2 > 0$, $p_2 = 0$ and $p_2 < 0$.

Case 1: $p_2 > 0$. The only positive solution to the equation (45) is given by

$$N_u^* = \frac{1}{2p_2}\left(p_1 + \sqrt{p_1^2 + 4\,\varepsilon p_2}\right), \tag{50}$$

where by straightforward analysis using (49) we can show that $N_u^* \leqslant 1$. We note that for $\varepsilon > 0$ the other root of the quadratic is negative.

In the biologically relevant limit of $\varepsilon \to 0$ there are three sub-cases depending on the sign of p_1. In the case of $p_1 > 0$, so that $\Psi > 0$, we have as $\varepsilon \to 0$ that

$$N_u^* \sim \frac{\Psi}{\Psi + \beta\lambda} - \varepsilon\,\frac{\beta^2\lambda^2\alpha}{\Psi(\Psi+\beta\lambda)^2}, \tag{51}$$

$$A^* \sim \frac{\Psi}{\alpha\lambda} + \varepsilon\,\frac{\beta}{\Psi}, \tag{52}$$

and for $p_1 = 0$, where $\Psi = 0$, we have

$$N_u^* \sim \varepsilon^{1/2} \left(\frac{\alpha}{\beta\lambda} \right)^{\frac{1}{2}} + \varepsilon^{3/2} \, \tfrac{1}{2} \left(\frac{\alpha}{\beta\lambda} \right)^{\frac{3}{2}}, \tag{53}$$

$$A^* \sim \varepsilon^{1/2} \left(\frac{\beta}{\alpha\lambda} \right)^{\frac{1}{2}} + \varepsilon \, \frac{1}{\lambda}, \tag{54}$$

for $\lambda > 0$; finally $p_1 < 0$, for which $\Psi < 0$, yields

$$N_u^* \sim \varepsilon \, \frac{\alpha}{(-\Psi)} - \varepsilon^2 \, \frac{\alpha^2(\beta\lambda - \Psi)}{(-\Psi)^3}, \tag{55}$$

$$A^* \sim \varepsilon \, \frac{\beta}{(-\Psi)} - \varepsilon^2 \, \frac{\alpha\beta^2\lambda}{(-\Psi)^3}, \tag{56}$$

as $\varepsilon \to 0$. The only regime in which solutions are not negligibly small as $\varepsilon \to 0$ is thus $p_1 > 0$, so that $\Psi > 0$, requiring the up-regulation rate to be sufficiently strong in comparison to the QSM sink terms. We further note from (52) that A^* is unbounded in the limit $\lambda \to 0$, so that $\Psi = 0$ marks the bifurcation between existence and non-existence of steady-state solutions when $\lambda = 0$, recalling from the remarks above that A grows linearly for $\Psi > 0$ or as a square root for $\Psi = 0$ as $t \to \infty$ in the $\lambda = 0$ case.

Case 2: $p_2 = 0$. Here, (45) reduces to a linear one giving

$$N_u^* = \frac{\varepsilon}{p_1} = \frac{\alpha\varepsilon}{\alpha\varepsilon + \beta\lambda}, \qquad A^* = \frac{\varepsilon}{\lambda}, \tag{57}$$

where clearly $0 < N_u^* \leqslant 1$; in the limit of $\varepsilon \to 0$ negligible up-regulation of cells is predicted.

Case 3: $p_2 < 0$. In this case, both solutions of (45) are positive, but only one solution satisfies $N_u^* \leqslant 1$, namely

$$N_u^* = \frac{1}{2p_2} \left(p_1 + \sqrt{p_1^2 + 4\,\varepsilon p_2} \right), \tag{58}$$

this being the smaller of the two roots. Series expansions of (58) in the limit $\varepsilon \to 0$ are given by (55) and (56).

We note that, except when $\lambda = 0$ or $\varepsilon = 0$, there is in each of the three cases one physical steady-state solution. In the (unphysical) case $\varepsilon = 0$ there are two physical roots; in the physically realistic limit $\varepsilon \to 0$ we need $\Psi > 0$ to obtain O(1) solutions for N_u^* and A^*, hence $\Psi = 0$ marks the bifurcation between successful and unsuccessful up-regulation to a quorate population. This would be reflected, using a biological example, by the success or failure for a population of *V. fischeri* in stationary phase to undergo bioluminescence. As discussed earlier, the experimental data suggest that α is significantly larger than β, λ and μ and O(1) densities of up-regulated cells are expected at steady state, implying that $\Psi > 0$ in practice.

The only case in which a steady state does not exist is when $\lambda = 0$ and $\Psi \geqslant 0$, whereby the QSM concentration continually grows and the up-regulated cell fraction is one. This is possible for cells grown in LB medium (Table 1) in which there is negligible QSM loss by the medium. In practice, however, QSM levels in LB tend to level off during the stationary phase (data not shown), which is probably due to QSM production being down-regulated in response to stresses induced by over-population.

5.3 *Linear stability analysis*

In this section we investigate whether the steady-state solution is physically realizable using linear stability analysis. In the usual way we take a perturbation from the steady-state solutions using

$$N_T \sim 1 + n_t, \quad N_u \sim N_u^* + n_u, \quad A \sim A^* + a,$$

where $n_t \ll 1, n_u \ll 1$ and $a \ll 1$. Substituting these expansions into (7) and (8), and linearizing yields the system

$$\begin{pmatrix} \mathrm{d}n_t/\mathrm{d}t \\ \mathrm{d}n_u/\mathrm{d}t \\ \mathrm{d}a/\mathrm{d}t \end{pmatrix} = \begin{pmatrix} F'(1) & 0 & 0 \\ F'(1)(\gamma - 1)N_u^* + \alpha A^* & -\alpha A^* - \beta & \alpha(1 - N_u^*) \\ \varepsilon - \mu A^* & 1 + \mu A^* - \varepsilon & -\mu(1 - N_u^*) - \lambda \end{pmatrix} \begin{pmatrix} n_t \\ n_u \\ a \end{pmatrix}. \tag{59}$$

To determine whether the perturbations n_t, n_u and a grow or decay in time, we seek the eigenvalues σ of the 3×3 matrix in (59). Substituting for A^* using (44), the characteristic equation can be written as

$$(F'(1) - \sigma)(\sigma^2 + Z_1(N_u^*)\,\sigma + Z_0(N_u^*)) = 0, \tag{60}$$

where

$$Z_1(N_u^*) = \mu(1 - N_u^*) + \lambda + \frac{\beta}{1 - N_u^*}, \tag{61}$$

$$Z_0(N_u^*) = \alpha\, p_2 \left(\frac{p_2 - p_1 - \varepsilon}{p_2} \frac{1}{(1 - N_u^*)} - (1 - N_u^*) \right). \tag{62}$$

For the steady state to be linearly stable, the real parts of all the roots of (45) must be negative. Since $F'(1) < 0$ implies that one root of the cubic is negative, then for the other roots to be negative requires that the coefficients of $Z_1(N_u^*)$ and $Z_0(N_u^*)$ must both be non-negative. Since physical solutions have $0 \leqslant N_u^* \leqslant 1$, it is clear that the coefficient $Z_1(N_u^*)$ will be positive. Defining $N_u^* = N_u^+$ and $N_u^* = N_u^-$ to be the larger and smaller roots of (45), respectively, it can be shown that

$$Z_0(N_u^\pm) = \pm \alpha p_2 (N_u^+ - N_u^-). \tag{63}$$

The stability of the steady-state solutions for each of the cases 1–3 are summarized as follows.

Case 1: $p_2 > 0$. In the case of $\varepsilon > 0$ the physical root is given by $N_u^* = N_u^+$ so $Z_0(N_u^+) > 0$. Hence both eigenvalues have negative real part and the steady state is stable. The other root $N_u^* = N_u^-$ and is a saddle point. In the case of $\varepsilon = 0$ there are two physical roots, namely $N_u^- = 0$ and $N_u^+ = \Psi/(\Psi + \beta\lambda)$; since we have $Z_0(0) < 0$ and $Z_0(N_u^+) > 0$, these are unstable and stable, respectively.

Case 2: $p_2 = 0$. The appropriate form for $Z_0(N_u^*)$ can be derived by taking the limit of $p_2 \to 0$ in (62) giving $Z_0(N_u^*) = \beta\lambda(1 - N_u^*) > 0$ and the steady-state solution is stable.

Case 3: $p_2 < 0$. In this case there are two positive roots, only one of which, namely $N_u^* = N_u^-$, is physical; since $p_2 < 0$ we have $Z_0(N_u^-) > 0$ and the physical root is again stable and the non-physical root is a saddle point.

In all cases the physical steady states are thus linearly stable. By examination of (7) and (8), it can easily be shown using a phase diagram that all trajectories starting within the physical range, i.e. $0 \leqslant N_T < 1, 0 \leqslant N_u < N_T$ and $0 \leqslant A < \infty$, will remain in this region tending to the steady-state solution. Consequently, these steady-state solutions are globally stable and will be attained whatever (physical) initial conditions are imposed. The uniqueness of a steady state solution as predicted by the model will be difficult to verify experimentally, as contrasting results, perhaps suggesting multiple steady states, may also occur due to the unavoidable minor differences in conditions between experiments. However, the model suggests that the quorum sensing process is robust and given suitable growth conditions (for example $\Psi > 0$ and $\varepsilon \ll 1$) the majority of the population will become up-regulated.

6. Discussion

In this paper we have introduced a simple mathematical model describing the phenomena occurring during the initial stages of quorum sensing in a population of bacteria. The model focuses on the activity and production of a single QSM and on its effects on a bacterial population consisting of cells in either of two states, corresponding to levels of gene activity depending on whether or not a QSM–QSP complex has bound to the *lux*-box, located on the chromosome. The basic assumptions of the model are thus based on known biological mechanisms and phenomena. The model assumes a well mixed population of cells, which is well suited to describing growth and production within batch culture experiments; best-fit parameters generally provide good quantitative agreement with the available experimental data. Furthermore, the rapid switch observed in experimental work from a colony of down-regulated cells to an up-regulated state is captured, the principle of the population needing to grow beyond a certain density for quorum sensing to occur being very well illustrated in Fig. 7. This feature falls quite naturally out of the model solutions, without having to impose threshold criteria within the model. Much of the quorum sensing literature speaks in terms of QSM reaching a critical concentration as inducing this rapid switch up-regulation of QSM production and behavioural change; however, the concept of a critical concentrations seems, in light of the known biology (for example, Fukua *et al.*, 1996) and of our model solutions to be artificial—the model solutions demonstrate that the observed behaviour is predicted without imposing such a switch. However, from a small initial population of down-regulated cells we observe from (1), using $G(A) = A$, that when

QSM levels reach $A \approx r/\alpha$ the growth and up-regulation terms are balanced. Hence as a rule of thumb a QSM concentration of r/α (where these are dimensional quantities) could be viewed as being the critical level.

In Sections 4 and 5 the main timescales and extent of up-regulation of cells was studied for the two main phases of bacterial growth in batch cultures, namely the exponential and stationary growth phases (see, for example Cano & Colomé, 1986, Chapter 6). The analysis of Section 4 reveals the important timescales of up-regulation of cells in an exponentially growing population in the limit $\kappa_d/\kappa_u = \varepsilon \to 0$ from a small colony of down-regulated cells (when the dimensionless quantities are of O(1) the relevant timescale is implicit in the non-dimensionalization). The analysis showed that the level of up-regulation remains very low until a time of around $\ln(1/\varepsilon)$, beyond which there are sufficient up-regulated cells to dominate QSM production. The value of the parameter Θ, which encompasses the rates of QSM production and of the down-regulation of up-regulated cells, is crucial in determining whether all the cells will become up-regulated cells. The bifurcation between total and partial up-regulation of cells, corresponding to exponential increase or levelling off of QSM concentration respectively, is given by $\Theta = 0$. Furthermore, increasing Θ reduces the timescale for the up-regulated cell fraction to become O(1), so that cells will become quorate earlier in the exponential phase. The analysis also provides indications as to why the dimensional parameters κ_d and β are difficult to pin down using the curve-fitting procedure. The data-fitted parameter values result in the parameter α being much the largest parameter in the system, which can be observed from the asymptotic analysis to be the dominant term governing the evolution of QSM and up-regulated cells during exponential growth. Consequently, the quantities $\beta \ll \alpha$ and $\varepsilon \ll 1$ can cover a wide range of values without having a significant effect on the solution. The analysis in Section 5 demonstrates that apart from two special cases, namely $\lambda = 0$ and $\varepsilon = 0$, there exists a single physical steady state for all non-negative parameter values. Moreover, the linear stability analysis in Section 5.3 shows that the physical solutions are stable (indeed they are globally stable to physical initial conditions) and are hence biologically realizable. The analysis in the limit $\varepsilon \to 0$ reveals the importance of parameter Ψ, which is related in some ways to Θ encompassing the rates of QSM production and loss through up-regulation, but also loss of QSM by the media. In suitable growth media Ψ is expected to be large (using the data in Table 1 suggests $\Psi = \mathrm{O}(10^3)$) implying that during the stationary phase of growth the vast majority of cells will be up-regulated. We note that the situation at the stationary phase is significantly more complex, where behavioural traits maybe switched on or off in response to the increased environmental stresses imposed at high population density (Golovlev, 1999); this is more than likely to effect the quorum sensing system, which the current model does not take into account. In practice, however, whether a population will become quorate will be highly dependent on a number of factors such as the growth media and temperature. These factors will be reflected by signs and magnitudes of the parameters Θ and Ψ.

Dockery & Keener (2001) modelled the quorum sensing process as a system of chemical reactions with exchange of QSMs via diffusion between the interior and exterior of each cell; cell density functions as a given parameter, rather than its time evaluation being calculated. This is different to the approach involving the switching on and off of genes used in our model. Both models demonstrate that increasing the cell density causes an increase in QSM production; however, the details of how this is achieved

are mathematically quite different. In Dockery & Keener (2001) the increase in QSM production as cell density increases results from moving along, and eventually jumping between, stable steady-state solutions along a hysteretic curve. In our model, by contrast, this behaviour occurs due to the cumulative effect of increased QSM inducing increased up-regulation as the population rises leading, providing Θ, $\Psi > 0$, to a relatively short timescale of rapid increase of QSM concentration which is faster than the population growth rate. Our modelling approach was guided by the requirement that parameter values be obtainable from routine experiments; the resulting model has fewer parameters than Dockery and Keener's, most of whose parameters are reaction rate coefficients for which values are currently unknown and will probably be very difficult to determine experimentally. An attractive advantage of our model is that cell densities and QSM concentrations can be readily determined experimentally, providing appropriate data for applying curve fitting procedures to our model, using, for example, the approach described in Section 2.2. Also, by considering explicitly two sub-populations of cells, we are able to predict systematically the proportion of cells that are up-regulated, providing a direct means of predicting, for example, the rates of virulence determinant production (e.g. for *P. aeruginosa*) or levels of light emission (e.g. for *V. fischeri*). Dockery and Keener extended their model to investigate spatio-temporal effects of quorum sensing in a chemostat. Spatio-temporal extensions to our model, investigating the role of quorum sensing in wound and biofilm situations, have also been developed and analysed; these results will be described in future publications.

The model only focuses on a single QSM and two bacterial states, but the biological reality can be very much more complicated. The mathematical model presented here is intended as a first step towards modelling more complex behaviour. Extensions to the model currently under investigation include the activation of phenotypes following up-regulation, the interaction of multiple QSMs and the role of QSM diffusion and of quorum sensing in biofilms and wound infections. The study of quorum sensing using simple mathematical models has the potential of providing valuable insights into a widespread phenomenon amongst bacteria which involves complex nonlinear couplings between a variety of species; such insights may not be achievable by experimental means. The implications of such quantitative understanding could be crucial in the design of new antibiotic or other therapies and of industrial processes.

Acknowledgements

J.P.W. gratefully acknowledges support by a Wellcome Trust Training Fellowship (fellowship ref. 054464/2/98) in Mathematical Biology and the other authors that of the BBSRC.

References

CANO, R. J. & COLOMÉ, J. S. 1986 *Microbiology*. West Publishing Company.

CROFT, J. C., WARD, J. P., KOERBER, A. J., WILLIAMS, P., KING, J. R. & SOCKETT, R. E. 2000 Microbiology and modelling of Pseudomonas wound infections. *Poster Presentation. American Society for Microbiology 100th General Meeting*. Los Angeles.

DOCKERY, J. D. & KEENER, J. P. 2001 A mathematical model for quorum sensing in *Pseudomonas aeruginosa*. *Bull. Math. Biol.*, **63**, 95–116.

DORING, G. 1993 *Pseudomonas aeruginosa* infection in cystic fibrosis patients. *Pseudomonas Aeruginosa as an Opportunistic Pathogen*. (M. Campa, M. M. Bendinelli & H. Friedman, eds), New York: Plenum Press.

EBERHARD, A. 1972 Inhibition and activation of bacterial luciferase synthesis. *J. Bacteriol.*, **109**, 1101–1105.

EBERHARD, A., BURLINGAME, A. L., EBERHARD, C., KENYON, G. L., NEALSON, K. H. & OPPENHEIMER, N. J. 1981 Structural identification of autoinducer of *Photobacterium fischeri*. *Biochem.*, **20**, 2444–2449.

EBERL, L., WINSON, M. K., STERNBERG, C., STEWART, G. S. A. B., CHRISTIANSEN, G., CHHABRA, S. R., BYCROFT, B., WILLIAMS, P., MOLIN, S. & GIVSKOV, M. 1996 Involvement of *N*-acyl-L-homoserine lactone autoinducers in controlling the multicellular behaviour of *Serratia liquefacians*. *Mol. Microbiol.*, **20**, 127–136.

EGLAND, K. A. & GREENBERG, E. P. 1999 Quorum sensing in *Vibrio fischeri*: elements of the *luxI* promoter. *Mol. Microbiol.*, **31**, 1197–1204.

FUQUA, W. C., WINANS, S. C. & GREENBERG, E. P. 1996 Census and concensus in bacterial ecosystems: the LuxR–LuxI family of quorum-sensing transcriptional regulators. *Ann. Rev. Microbiol.*, **50**, 727–751.

GOLOVLEV, E. L. 1999 An introduction to the biology of the stationary-phase of bacteria: the mechanism of the common response to stresses. *Microbiol.*, **68**, 543–550.

HOLDER, I. A. 1993 *Pseudomonas aeruginosa* burn infections: pathogenesis and treatment. *Pseudomonas Aeruginosa as an Opportunistic Pathogen*. (M. Campa, M. M. Bendinelli & H. Friedman, eds), New York: Plenum Press.

JAMES, S., NILSSON, P., JAMES, G., KJELLEBERG, S. & FAGERSTRÖM, T. 2000 Luminescence control in the Marine Bacterium *Vibrio fischeri*: an analysis of the dynamics of *lux* regulation. *J. Mol. Biol.*, **296**, 1127–1137.

KAPLAN, H. B. & GREENBERG, E. P. 1985 Diffusion of autoinducer is involved in the regulation of the *Vibrio fischeri* luminescence system. *J. Bacteriol.*, **163**, 1210–1214.

MCCLEAN, K. H., WINSON, M. K., FISH, A., TAYLOR, A., CHHABRA, S. R., CAMARA, M., SWIFT, S., LAMB, J., BYCROFT, B. W., STEWART, G. S. A. B. & WILLIAMS, P. 1997 Quorum sensing in *Chromobacterium violeceum*: exploitation of violacein production and inhibition for the detection of *N*-acylhomoserine lactones. *Microbiology*, **143**, 3703–3711.

MCKNIGHT, S. L., IGLEWSKI, B. H. & PESCI, E. C. 2000 The *Pseudomonas* quinolone signal regulates *rhl* quorum sensing in *Pseudomonas aeruginosa*. *J. Bacteriol.*, **182**, 2702–2708.

MEIGHEN, E. A. 1991 Molecular biology of bacterial bioluminescence. *Microbiol. Rev.*, **55**, 123–142.

NEALSON, K. H., PLATT, T. & HASTINGS, J. W. 1970 Cellular control of the synthesis and activity of the bacterial luminescent system. *J. Bacteriol.*, **104**, 313–322.

PEARSON, J. P., VAN DALDEN, C. & IGLEWSKI, B. H. 1999 Active efflux and diffusion are involved in transport of *Pseudomonas aeruginosa* cell-to-cell signals. *J. Bacteriol.*, **181**, 1203–1210.

PIPER, K. R., BECK VON BODMAN, S. & FERRAND, S. K. 1993 Conjugation factor of *Agrobacterium tumefacians* regulates Ti plasmid transfer by autoinduction. *Nature*, **362**, 448–450.

RUMBAUGH, K. D., GRISWOLD, J. A., IGLEWSKI, B. H. & HAMOOD, A. N. 1999 Contribution of quorum sensing to the virulence of *Pseudomonas aeruginosa* in burn wood infections. *Infect. Immun.*, **67**, 5854–5862.

SALMOND, G. P. C., BYCROFT, B. W., STEWART, G. S. A. B & WILLIAMS, P. 1995 The bacterial 'enigma': cracking the code of cell–cell communication. *Mol. Micriobiol.*, **16**, 615–624.

SWIFT, S., THROUP, J. P., WILLIAMS, P., SALMOND, G. P. C. & STEWART, G. S. A. B. 1996 Quorum sensing: a population density component in the determination of bacterial phenotype. *Trends Biochem. Sci.*, **21**, 214–219.

WILLIAMS, P., BAINTON, N. J., SWIFT, S., CHHABRA, S. R., WINSON, M. K., STEWART, G. S. A. B., SALMOND, G. P. C. & BYCROFT, B. W. 1992 Small molecule-mediated density dependent control of gene expression in prokaryotes: bioluminescence and the biosynthesis of carbapenum antibiotics. *FEMS Microbiol. Lett.*, **100**, 161–168.

WILLIAMS, P., CAMARA, M., HARDMAN, A., SWIFT, S., MILTON, D., HOPE, V. J., WINZER, K., MIDDLETON, B., PRITCHARD, D. I. & BYCROFT, B. W. 2000 Quorum sensing and the population-dependent control of virulence. *Phil. Trans. R. Soc. Lond.* B, **355**, 1–14.